VHF Single Crystal Silicon Capacitive Elliptic Bulk-Mode Disk Resonators—Part II: Implementation and Characterization

Siavash Pourkamali, *Student Member, IEEE*, Zhili Hao, *Member, ASME*, and Farrokh Ayazi, *Member, IEEE*

***Abstract*—This paper, the second of two parts, reports on the implementation and characterization of high-quality factor (Q) side-supported single crystal silicon (SCS) disk resonators. The resonators are fabricated on SOI substrates using a HARPSS-based fabrication process and are 3 to 18 μm thick. They consist of a single crystal silicon resonant disk structure and trench-refilled polysilicon drive and sense electrodes. The fabricated resonators have self-aligned, ultra-narrow capacitive gaps in the order of 100 nm. Quality factors of up to 46 000 in 100 mTorr vacuum and 26 000 at atmospheric pressure are exhibited by 18 μm thick SCS disk resonators of 30 μm in diameter, operating in their elliptical bulk-mode at $\sim$150 MHz. Motional resistance as low as 43.3 kΩ was measured for an 18-μm-thick resonator with 160 nm capacitive gaps at 149.3 MHz. The measured electrostatic frequency tuning of a 3-μm-thick device with 120 nm capacitive gaps shows a tuning slope of -2.6 ppm/V. The temperature coefficient of frequency for this resonator is also measured to be -26 ppm/°C in the temperature range from 20 to 150 °C. The measurement results coincide with the electromechanical modeling presented in Part I. [1224]**

***Index Terms*—HARPSS, microresonator, quality factor, silicon-on-insulation (SOI), temperature coefficient.**

I. Introduction

DEVELOPMENT of integrated silicon-based micromechanical resonators with high frequencies and high quality factors can have a great impact on the future of wireless communication systems by providing on-chip replacement to the off-chip and bulky frequency-selective components in such systems. A significant amount of research is currently underway to extend the operating frequency of micromechanical resonators into the VHF and UHF range. Extension of the operating frequency of capacitive MEMS resonators into high frequency range, while maintaining acceptable power handling capability and low impedance level, requires large transducer capacitances. This in turn calls for reproducible manufacturing technologies that can increase the capacitive area and reduce the inter-electrode capacitive gaps to a few tens of nanometers [1]. Therefore, fabrication technologies that can implement *thick* high-Q capacitive resonators with *scalable nanometer-in-size* interelectrode gap spacing without the need for nanolithography are of great interest.

A variety of high frequency micromechanical resonators with single crystal or polycrystalline silicon as the structural material have been reported in literature. VHF and UHF capacitive MEMS resonators with polysilicon as the structural material and submicron gap spacing have been implemented using surface micromachining techniques [2], [3]. Single crystal silicon (SCS) is a superior structural material for microresonators compared to polysilicon due to its inherent high mechanical quality factor [4], lower internal stress and independence from various process parameters. However, since SCS cannot be deposited using conventional chemical vapor deposition (CVD) techniques, fabrication of electrically isolated SCS structures with ultranarrow (<100 nm) capacitive gaps for high-frequency applications using conventional lithography is not a trivial task. High-frequency capacitive SCS resonators that have been so far reported have large lithography defined sense and drive capacitive gaps [5] that are not suitable for operation in the VHF and UHF range. Comparing to piezoelectrically operated SCS resonators [6] where the sense and drive electrodes are in direct physical contact with the resonating body, adding excessive surface and support loss to the structure, capacitive resonators exhibit much higher quality factors.

This work presents implementation and characterization of high-Q and high-frequency ($Q > 10\,000, f > 100$ MHz) SCS bulk-mode capacitive resonators. A fabrication technology based on the HARPSS process [7], [8] has been developed to implement thick SCS bulk-mode disk resonators with sub 100–200 nm capacitive gaps on SOI substrates. Sub-100 nanometer self-aligned vertical capacitive gaps between 18 μm thick SCS resonators and polysilicon electrodes are demonstrated. Thick bulk-mode resonators with in-plane vibrations have the advantage of providing larger drive and sense area by extending in the vertical direction into the silicon substrate. Larger transduction area will reduce the equivalent motional resistance of the resonator when combined with the ultra-narrow gaps and high quality factor provided by the SCS resonating element. This in turn will facilitate insertion of such devices in RF systems by providing matching capability and increasing the signal to noise ratio. Details of the experimental results on the resonant frequencies and quality factors of side-supported disk resonators operating in their elliptical bulk-mode are provided in this paper. Motional resistance, electrostatic tuning and temperature characteristics of the fabricated disk resonators are also investigated. The measured results show good agreement

Manuscript received December 10, 2003; revised February 3, 2004. This work was supported by DARPA under Contract DAAH01-01-1-R004. Subject Editor G. Stemme.

The authors are with the School of Electrical and Computer Engineering, Georgia Institute of Technology, Atlanta, GA 30332-0250 USA (e-mail: farrokh.ayazi@ece.gatech.edu).

Digital Object Identifier 10.1109/JMEMS.2004.838383

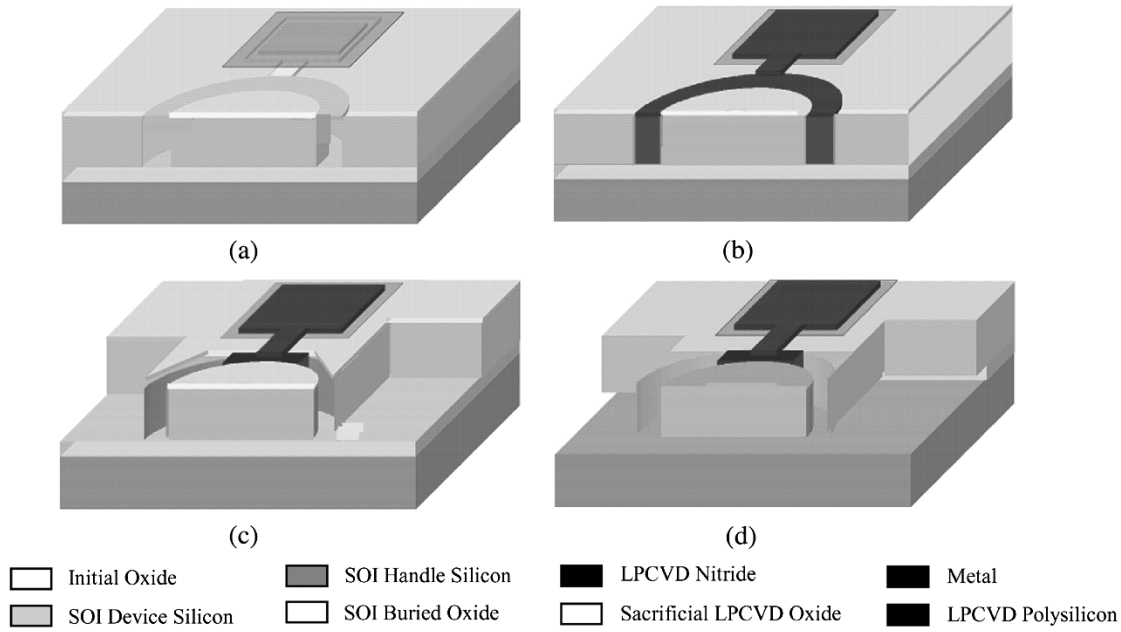

Fig. 1. Fabrication process flow of single crystal silicon resonators with sub-100 nm gaps on SOI. (a) Grow and pattern initial oxide, deposit and pattern LPCVD nitride, etch trenches (Bosch process). (b) Grow and remove thin oxide (surface treatment), deposit and blanket etch sacrificial oxide, deposit and pattern doped LPCVD polysilicon. (c) Pattern initial oxide, metallization, etch release openings and pattern polysilicon for electrodes. (d) HF release and undercut.

with the theoretical analysis and model presented in Part I of this work.

II. Resonator Fabrication

In this work, a variation of the HARPSS process [9] has been developed to fabricate bulk-mode, VHF SCS capacitive MEMS resonators *on SOI substrates*. It represents the first SOI implementation of the HARPSS process. The advantages of using an SOI substrate compared to a regular silicon substrate used previously to implement low frequency SCS beam resonators [10] are: 1) The ability to achieve "electrical isolation" between the body of individual SCS resonators in an array implementation (e.g., for filter synthesis), which provides independent tuning capability for the resonators as well as reducing the parasitic capacitances and the related cross-talk, 2) enabling nano-precision fabrication of "bulk-mode" SCS resonators with height-to-width-ratio <1 (e.g., disks and blocks) for high-frequency operation (VHF and UHF); perfect dimensional definition of such devices on regular silicon substrates is not possible due to the uncertainty caused by the isotropic silicon etch step to undercut and release the structures at the bottom; and 3) In the earlier implementation of HARPSS SCS resonators on regular silicon substrates, the sacrificial oxide was used as a protective layer for the silicon structures during the isotropic etch step [10]. Due to finite selectivity of the SF6 silicon plasma etch to oxide, the minimum achievable gap size was therefore limited by this mechanism. The use of SOI eliminates the need for isotropic silicon etching and hence the capacitive gaps can be reduced to their true physical limits.

The processing steps for fabrication of SCS HARPSS resonators on SOI substrates is shown in Fig. 1. The fabrication process consists of six lithography steps and a number of etching and deposition steps. Fabrication flow starts with growing a 1-μm-thick layer of initial oxide on the SOI substrate.

The initial oxide is kept on the input and output wirebonding pads as well as the resonating body of the resonators while it is removed on the rest of the area using plasma etching. The patterned initial oxide serves as: 1) an insulating layer to provide isolation between the substrate and the input and output wirebonding pads; 2) a mask for the subsequent silicon trench etching step which defines the resonating SCS structures. A thin layer of LPCVD silicon nitride $(\sim 3000\ \text{Å})$ is then deposited. The nitride layer is to be patterned on the pad area to protect the pad oxide during the HF release step at the end of the process. It is worth noting that due to existence of patterned oxide features on the substrate, anisotropic plasma etching of nitride will result in undesired nitride residues on the edges of the resonators. This can be explained by the fact that the deposited nitride layer has a higher effective vertical thickness at the oxide steps. To avoid the undesired nitride residues, the nitride layer is wet etched isotropicaly in phosphoric acid. A thin layer $(\sim 5000\ \text{Å})$ of LPCVD high-temperature oxide (HTO) patterned in buffered HF (BHF) is used as a mask for nitride wet etching.

The SCS resonating elements are defined by etching trenches in the device layer all the way down to the buried oxide layer of the SOI in a deep-reactive ion etching (DRIE) system using the Bosch process. The thickness of the SOI device layer determines the thickness of the resonators and can be as thick as a few tens of microns. Due to high selectivity of the SF_6 silicon etching plasma used in the inductively coupled plasma (ICP) system to oxide and nitride (>100), the patterned oxide and nitride layers are used as the protecting mask layer for silicon.

As reported in [11], reduction of the surface roughness of the resonator sidewalls and removing the damaged surface caused by plasma can slightly improve the quality factor of SCS beam

resonators. On the other hand for ultra-narrow (<100 nm) capacitive gaps, the rough resonator sidewalls may result in large local electric fields when the polarization voltage is applied between the resonator and the electrodes. Large local electric fields may in turn cause undesired leakage current through tunneling-based mechanisms [12]. Therefore after etching the trenches, a thin layer of thermal oxide (1000–2000 Å) is grown and subsequently removed in BHF. A thin layer of LPCVD high-temperature sacrificial oxide (HTO), conformally covering all the resonator sidewalls is then deposited at 850 °C. The thickness of the deposited sacrificial oxide layer, determines the capacitive gap size between the polysilicon electrodes and the SCS resonator and can be 10 s of nanometer up to a few microns (90–160 nm in this work).

The sacrificial oxide is removed on the surface by a short anisotropic oxide plasma etching, while keeping it on the resonator sidewalls, so that the deposited polysilicon for the pads will be in direct contact with the nitride layer and remains firmly anchored during the HF release. Trenches are subsequently refilled with doped LPCVD polysilicon to form the vertical electrodes. The deposited polysilicon (~ 3 μm thick) is patterned on the surface to form the wirebonding pads for the input and output electrodes.

Metallization is performed afterwards and a thin layer of metal (Cr: 300 Å/Au: 2000Å) is deposited on the wirebonding pads in an e-beam evaporator system to promote adhesion and electrical conductivity between the wirebonds and the polysilicon pads.

Release openings are then etched in the silicon device layer and the polysilicon inside the trenches is simultaneously patterned to form the electrodes. The resonators are then released from the handle silicon layer and the electrodes by removing the buried oxide layer (BOX) of the SOI and the sacrificial oxide in an HF:H_2O solution. BOX thickness for the substrates used in this work was 2 μm. Generally, larger BOX thickness has the advantage of lower parasitics to the handle substrate and shorter undercut time. In addition stiction of compliant structures to the handle substrate is an issue for small BOX thickness (<1 μm) and thin device layers (<3 μm).

A number of side-supported SCS disk resonators with various designs (i.e., number of supports and electrodes) and different thickness were fabricated using the described fabrication sequence on SOI substrates. For single support resonators if the support beam does not have large enough lateral stiffness (long and thin support beams) stiction to the electrodes may be an issue, however for the resonators demonstrated in this work stiction was not observed.

Fig. 2 shows the SEM view of a fabricated 18 μm thick, 49.5 μm in diameter SCS disk resonator. The disk resonator is supported from the sides at two opposite resonance nodes and has 90 nm capacitive gaps between its SCS resonating body and sense and drive polysilicon electrodes.

Fig. 3 shows a fabricated 3 μm thick, 29.4 μm in diameter SCS disk resonator supported at only one of its resonance nodes with 120 nm capacitive gaps.

Fig. 4 is the close-up view of the electrode area for a fabricated disk resonator showing the SCS disk, the polysilicon electrode and the 90 nm capacitive gap in between.

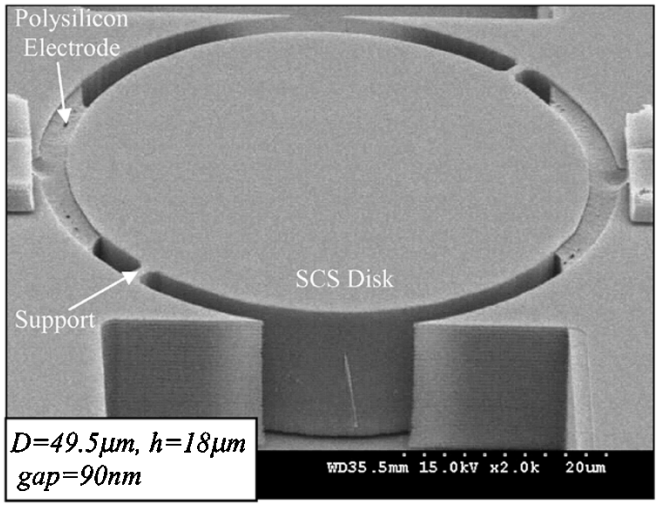

Fig. 2. SEM of a 49.5 μm in diameter, 18 μm thick, side-supported SCS disk resonator with two supports and a capacitive gap spacing of 90 nm.

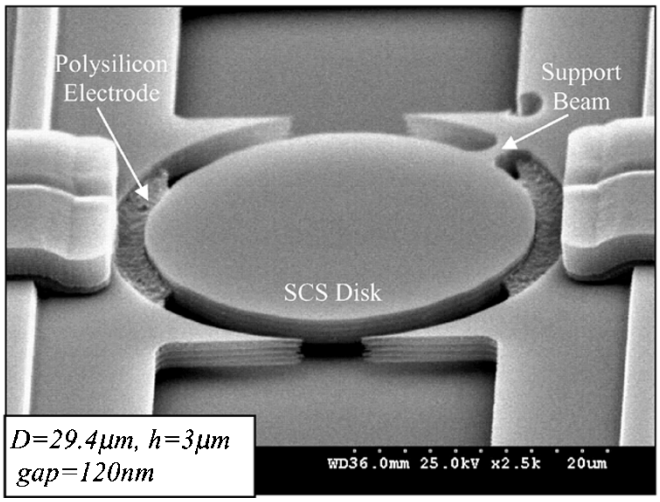

Fig. 3. SEM of a 29.4 μm in diameter, 3 μm thick, side-supported SCS disk resonator supported with only one support beam and a capacitive gap spacing of 120 nm.

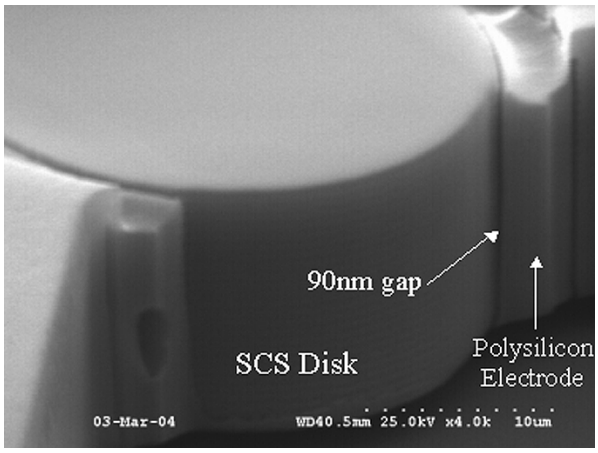

Fig. 4. Close-up view of the electrode area for a fabricated disk resonator showing the 90 nm gap spacing between the polysilicon electrode and the SCS disk resonator.

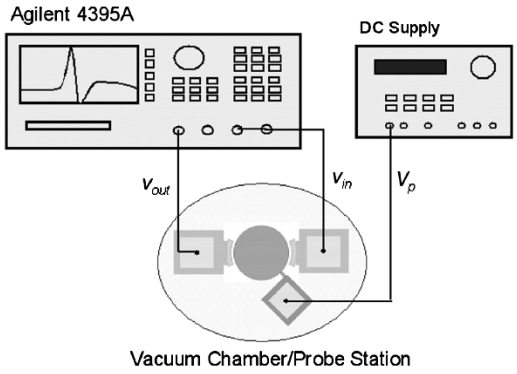

Fig. 5. Schematic diagram of the test setup for measurement of high-frequency resonators.

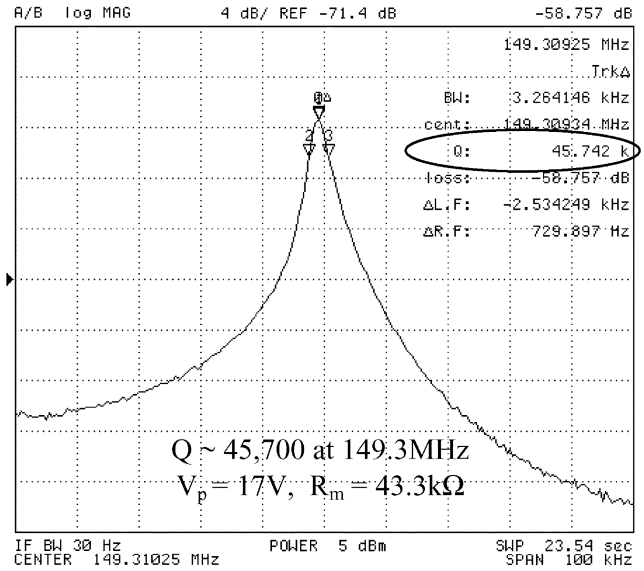

Fig. 6. Frequency response of a 29.2-μm-diameter, 18-μm-thick SCS disk resonator supported at one resonance node.

III. Performance Characterization and Verification

A. Center Frequency and Quality Factor Measurement

A few of the fabricated side-supported disk resonators with different number of support beams and various dimensions were tested both under vacuum and atmospheric pressure. The experimental setup used for measurement is illustrated in Fig. 5. The MEMS resonator chip was mounted on a board and the input and output signals along with the dc polarization voltage were applied to the resonator through wirebonds. The resonators were connected directly to the network analyzer (Agilent 4395A) in a two-port configuration via coaxial cables.

Fig. 6 is the frequency response of a 29.2-μm-diameter, 18-μm-thick disk resonator in vacuum showing a quality factor of 45 700 for the elliptical bulk-mode of this resonator at 149.3 MHz. This is one of the highest Q-frequency products (6.8×10^{12}) reported to date for capacitive micromechanical resonators, and is 40 times larger than the highest achieved Q-frequency products for the flexural mode SCS HARPSS beam resonators.

The SEM view of this resonator is shown in Fig. 7. The disk is supported by a 1.2-μm-wide, 4-μm-long support beam *at only one resonant node* and has four electrodes for actuation and sensing. Each pair of confronting electrodes is electrically connected. The polysilicon beam bridging over the resonator provides electrical connection between two of the electrodes, while the other pair of electrodes are connected by a silicon trace extending around the device [see Fig. 7(a)]. The capacitive gap size for this resonator is 160 nm.

Fig. 8 shows frequency response of the same resonator in air showing a quality factor of 25 900, which is the highest reported quality factor for a VHF silicon micromechanical resonator under atmospheric pressure so far. Unlike lower frequency beam resonators, the Q of ultrastiff bulk-mode resonators (i.e., disks) is much less susceptible to the pressure of the surrounding environment [2]–[13]. Due to much higher stiffness of such resonators, the ratio of the energy lost by the air damping to the stored energy in the resonator is much smaller compared to that of the flexural mode of lower frequency beam resonators. Such high quality factor in the atmospheric pressure shows the potential of such devices for several applications without the need for expensive vacuum packaging.

Fig. 9 illustrates the frequency response of the 29.4-μm-diameter, 3-μm-thick disk resonator of Fig. 3 under 100 mtorr vacuum. The disk is supported by a 1.7-μm-wide, 2.7-μm-long support beam at only one resonant node. A quality factor of 39 300 has been measured under vacuum for the elliptical bulk-mode of this resonator at 147.8 MHz.

The resonant frequency calculated by (1) developed in part I for the elliptical bulk-mode of a disk resonator with such dimensions is 148.3 MHz.

$$f_m = \frac{k_m}{2\pi R} \cdot \sqrt{\frac{E}{\rho \cdot (1-\upsilon^2)}}. \tag{1}$$

It is worth noting that the disk resonators in this work are fabricated on $\langle 100 \rangle$ silicon substrates and the electrodes are aligned to the $\langle 110 \rangle$ orientation (along the maximum Young's modulus). Therefore, since the maximum flexing happens along the $\langle 110 \rangle$ orientation, mechanical properties of silicon along the $\langle 110 \rangle$ orientation are used in (1) for calculating the resonant frequency. Due to the higher Young's modulus and lower Poisson's ratio along the $\langle 110 \rangle$ orientation in silicon compared to those along $\langle 100 \rangle$, 22% higher resonant frequencies can be achieved by aligning the disk resonators to the $\langle 110 \rangle$ orientation instead of $\langle 100 \rangle$, as confirmed by the ANSYS simulations presented in part I. Finite element analysis for a disk resonator of such dimensions was presented in part I (considering the anisotropy of SCS), showing a resonant frequency of 148 MHz for the elliptical bulk-mode in operation. Therefore, the measured data is in excellent agreement with the theory and numerical simulation.

The 29.4-μm disk resonator was also operated in atmospheric pressure and demonstrated a quality factor of 8 200, as shown in Fig. 10. Smaller capacitive gap size of the 3 μm thick resonator (120 nm) comparing to its 18-μm-thick counterpart (160 nm) is suspected to be the reason behind its lower quality factor in air.

Fig. 11 shows the frequency response of a 49.5-μm-diameter, 3-μm-thick disk resonator having four supports (each is 0.7 μm wide and 2.7 μm long) at its four resonant nodes. The SEM picture of this device is shown in Fig. 12. A quality factor of 6 400

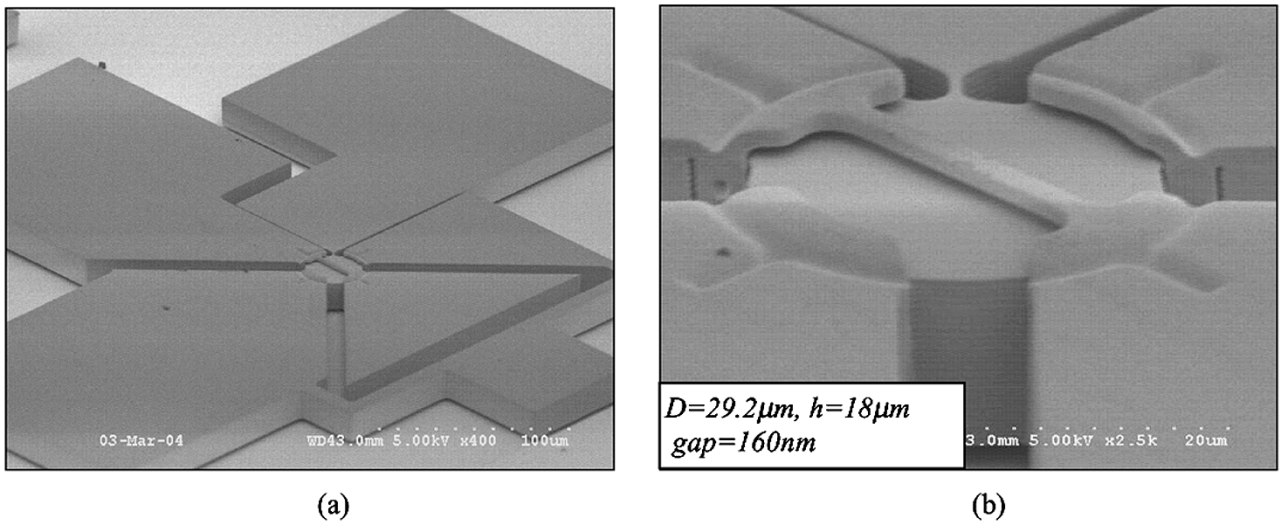

Fig. 7. SEM of the 29.2-μm-diameter, 18-μm-thick SCS disk resonator supported at one resonance node. (a) Full view of the device and (b) close-up of the disk and electrodes. Gap Size = 160 nm.

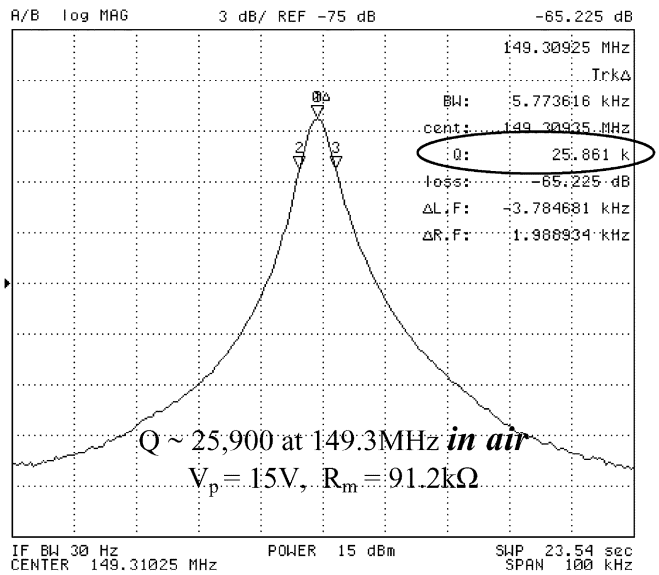

Fig. 8. Frequency response of the 18-μm-thick, 29.2-μm-diameter disk resonator of Fig. 9 in air.

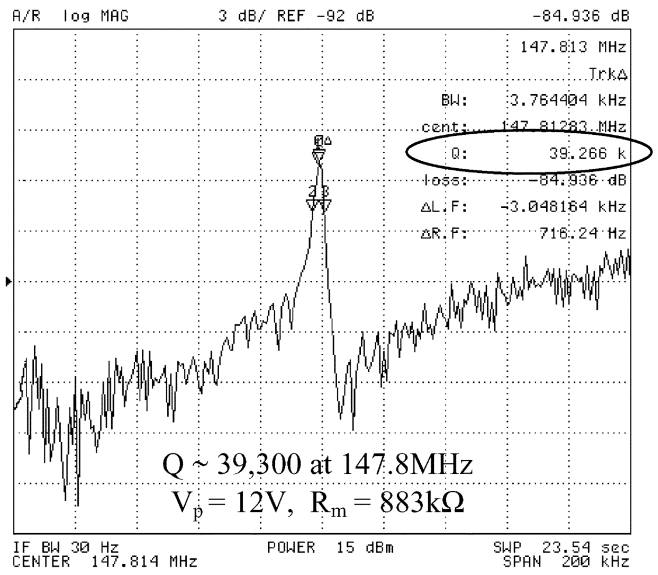

Fig. 9. Frequency response of a 29.4-μm-diameter, 3-μm-thick SCS disk resonator supported at one resonance node.

was measured for this resonator under vacuum at center frequency of 87.7 MHz corresponding to its elliptical bulk mode. Equation (1) predicts a resonant frequency of 88.1 MHz for this resonator. Much lower quality factor measured for this resonator comparing to the singly supported disks suggests that support loss is the major loss mechanism in side supported disk resonators. Each support acts as an energy sink to the substrate, therefore the quality factor of the resonators increases dramatically by reducing the number of supports.

B. Motional Resistance

From a system design perspective, motional resistance is one of the most critical parameters of a micromechanical resonator. At its resonant frequency, the resonator is equivalent to an electrical resistance terminated by two parallel capacitors to ground. When testing, the resonators were directly connected to the 50 Ω input and output impedance of the network analyzer and the impedance of the terminating capacitors that are typically much higher than 50 Ω can be neglected. Therefore, the value of the equivalent motional resistance of the resonators can be extracted from the frequency response plots using (2)

$$R_{\mathrm{eq}} = 50 \times 10^{\frac{\mathrm{I.L.}}{20}} \tag{2}$$

where I.L. is the measured insertion loss of the resonator at its resonant frequency. The motional resistance values extracted from the frequency response plots of the resonators (Figs. 6, 8–11) are 1.327 MΩ for the 88 MHz resonator with polarization voltage of 17 V, and 0.883 MΩ and 2.073 MΩ for the 148 MHz resonator in vacuum ($\mathrm{V_p} = 12$ V) and air ($\mathrm{V_p} = 17$ V), respectively. For the 18-μm-thick resonator, larger device thickness and more number of electrodes surrounding all around the disk, provides much larger area for actuation and sensing of the resonator. Therefore, despite having larger capacitive transducer

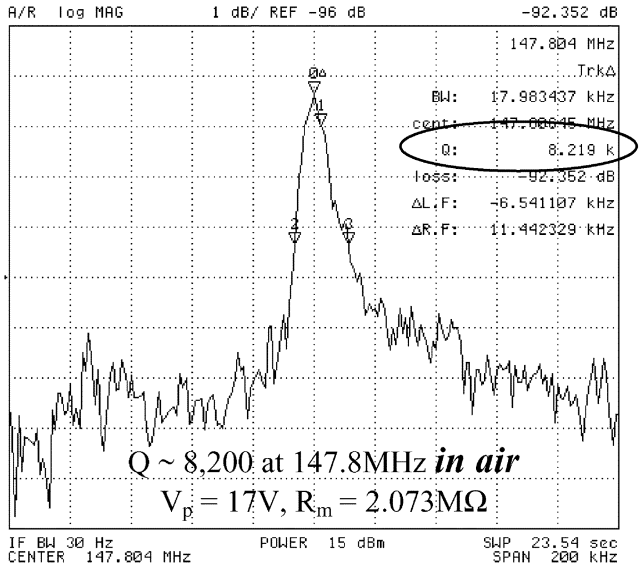

Fig. 10. Frequency response of the 29.4-μm-diameter disk resonator of Fig. 3 in air.

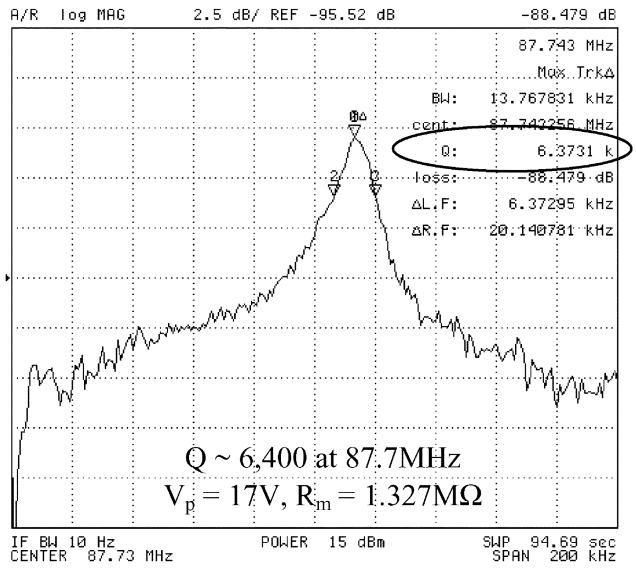

Fig. 11. Frequency response of a 49.5-μm-diameter, 3-μm-thick SCS disk resonator supported at four resonance nodes.

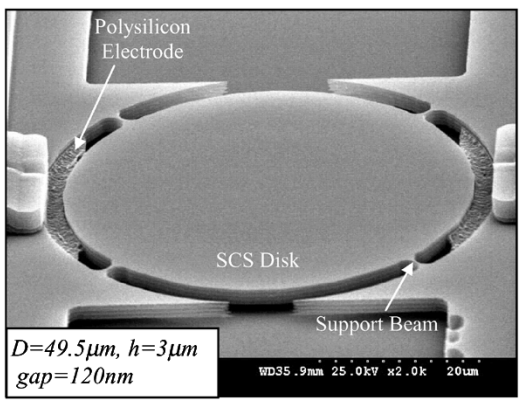

Fig. 12. SEM of the 49.5-μm-diameter, 3-μm-thick, SCS disk resonator supported at its four resonance nodes. Gap Size = 120 nm.

gaps, more than one order of magnitude smaller motional resistance and larger signal to noise ratio has been achieved for the resonator (43.3 kΩ in vacuum with $V_p = 17$ V, and 91.2 kΩ with $V_p = 15$ V in air).

The theoretical model of Part I for motional resistance has been used to calculate the motional resistance values for comparison with the measurement results. The measured quality factors, have been used to calculate the equivalent motional resistances. Table I summarizes the calculated motional resistances and resonator parameters as well as measured quality factors and motional resistances for the disk resonators. The vibration amplitudes are also calculated from the model and are listed in Table I. The calculated vibration amplitudes are in the range of a few nanometer. Taking into account fabrication tolerances and measurement inaccuracies, the theoretical model is in good agreement with the measured characteristics of the resonators and can be used as a reliable tool for prediction of the dynamic behavior and design of the capacitive disk resonators.

C. Electrostatic Frequency Tuning

Fig. 13 shows the measured electrostatic frequency-tuning characteristic for the 3-μm-thick, 29.4-μm-diameter disk resonator, showing a frequency tuning range of 1.9 kHz by changing the polarization voltage from 10 to 15 V. Equation (3), derived in Part I, shows the effect of the electrical stiffness caused by the polarization voltage on the resonant frequency of the elliptical mode disk resonators

$$f_{\text{tuned}} = f \cdot \sqrt{1 - \varepsilon \cdot h \cdot R \cdot \left(\frac{\theta_e}{2} + \frac{\sin(2\theta_e)}{4}\right) \cdot V_p^2 \cdot [2/d^3]/K} \tag{3}$$

By taking the derivative of the tuned frequency versus the polarization voltage, the following expression for the frequency tuning slope can be obtained:

$$\frac{\partial f_{\text{tuned}}}{\partial V_p} = -\frac{2 V_p f \varepsilon A_e}{K d^3} \tag{4}$$

where A_e is the effective electrode area and is given by (5)

$$A_e = h \cdot R \cdot \left(\frac{\theta_e}{2} + \frac{\sin(2\theta_e)}{4}\right). \tag{5}$$

Using (4) and (5), and the measured tuning slope of -2.6 ppm/V, an effective capacitive gap size of 120 nm is extracted for the disk resonator, which accurately coincides with the actual measured capacitive gaps of the resonator.

D. Temperature Coefficient of Frequency

The temperature-induced frequency drift of the 147.8 MHz disk resonator was measured in vacuum using a RF vacuum probe station with temperature control capability. As shown in Fig. 14, the measured frequency drift has a linear trend with a slope of -26 ppm/°C over the 20–150°C temperature range. Based on the discussion in Part I, the frequency drift is mainly due to the temperature dependence of Young's modulus of silicon. From the measured frequency drift, a temperature coefficient of -55 ppm/°C is determined for the Young's modulus of highly p-type doped SCS.

TABLE I
CALCULATED AND MEASURED PARAMETERS OF THE CAPACITIVE DISK RESONATORS OPERATING IN ELLIPTICAL BULK-MODE

Parameter	Device 1		Device 2		Device 3
Diameter (μm)	29.4		29.2		49.5
Thickness (μm)	3		18		3
Drive and sense gaps (nm)	120		160		120
Operating condition	vacuum	air	vacuum	air	
Bias voltage (V)	12	17	17	15	17
Drive voltage (V)	1.26	1.26	0.398	1.26	1.26
Quality factor	39,266	8,219	45,742	25,861	6,373
Vibration Amplitude (Am/R, nm)	4.5	1.4	3.1	4.9	2.1
Measured motion resistance (kΩ)	883	2073	43.3	91.2	1327
Calculated motion resistance (kΩ)	756	1798	42.6	96.7	1382

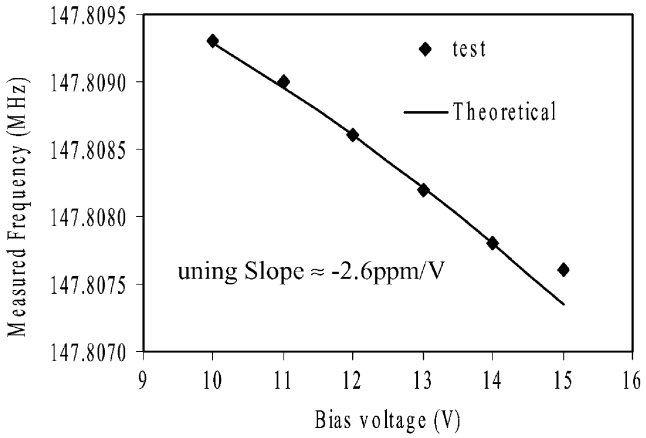

Fig. 13. Measured and calculated electrical tuning characteristic for the 147.8 MHz disk resonator showing an effective capacitive gap size of 120 nm for the device.

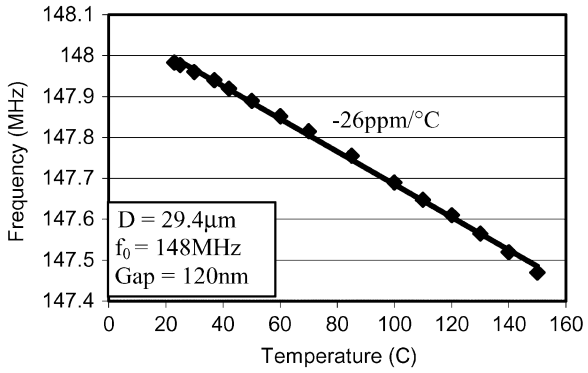

Fig. 14. Measured temperature characteristics of frequency for the 148 MHz side supported disk resonator showing a linear frequency drift profile with a slope of -26 ppm/°C.

IV. DISCUSSIONS

A. Motional Resistance

The major bottleneck for implementation of high frequency capacitive resonators that can be used as RF system components is the large equivalent motional resistance and low power handling capability of such devices. As shown in Part I, the equivalent electrical resistance of a capacitive elliptical mode disk resonator is given by (6):

$$R_{21} = \frac{\sqrt{K \cdot M}}{Q \cdot \eta_1 \cdot \eta_2}. \tag{6}$$

Replacing η_1 and η_2 with the related resonator parameters and assuming symmetry for the device (identical sense and drive electrodes), (6) gives rise to (7)

$$R_{21} = \frac{\sqrt{KM}d^4}{Q\varepsilon_0^2 L_{\text{eff}}^2 h^2 V_p^2} \propto \frac{d^4}{Q \cdot h} \tag{7}$$

where L_{eff} is the effective length of the electrodes, and is given by (8).

$$L_{\text{eff}} = R \cdot \sin(\theta_e) \tag{8}$$

According to (7), the motional resistance of the device is determined by the mechanical properties of the resonator as well as the electromechanical coupling between the transducer electrodes and the resonator. The electromechanical coupling is in turn a function of the sense and drive electrodes effective area $(L_{\text{eff}} \times h)$, capacitive gap size (d) in between the electrodes and the resonator, and the applied dc polarization voltage (V_p). As evident, ultranarrow capacitive gaps, high Q and large electrode area are needed to maintain reasonably low equivalent electrical resistance for the RF MEMS capacitive resonators as their dimensions are scaled down to achieve higher operating frequencies. Achieving smaller equivalent resistance facilitates insertion of the resonators in various high frequency systems, i.e., bandpass filters [14], by providing the capability of impedance matching to the $50\ \Omega$ nominal impedance of RF components.

B. HARPSS Fabrication Technology

As far as the motional resistance of the resonators is concerned, reasonably low motional resistances can be achieved for high-frequency HARPSS capacitive resonators. The capacitive gaps of HARPSS resonators are determined in a self-aligned manner by the thickness of a sacrificial oxide layer and can be reduced to their smallest physical limits (10's of nanometers) independently from the lithography limits. In addition, the thickness of the SCS HARPSS resonators can be increased to a few 10's of microns while keeping the capacitive gaps in the nanometer scale, resulting in a lower equivalent motional resistance compared to their surface micromachined polysilicon counterparts with thickness limited to 1–3 μm[2]–[4]. Larger device thickness also improves power-handling capability of the resonators. Finally, the all-silicon resonators with *SCS* as the resonating element exhibit high-Q and good long-term stability.

As an example, for the 148 MHz disk presented in this work, by reducing the capacitive gap sizes to 30 nm, increasing the

device thickness to 20 μm, and maximizing the electrode area (having four electrodes all around the resonator) the motional resistance will be reduced to 130 Ω. At the same time the electrostatic tuning slope for such resonator will increase to -260 ppm/V, which is large enough to compensate the temperature dependent frequency drift of the device by changing the polarization voltage.

C. Disk Thickness

As it was mentioned and demonstrated practically, the disk resonators implemented using the HARPSS technology have the potential to decrease motional resistance by increasing the thickness of the resonating structure. However, when the disk thickness and diameter are comparable in size, the coupling between the in-plane vibration modes and thickness modes comes to the fore [15], [16]. Therefore, the effect of the disk thickness on the in-plane vibrations should be addressed here.

As described in Part I, the formula for the resonant frequencies and mode shapes of the in-plane vibrations of a disk resonator are derived with the assumption that the disk thickness is much smaller than its diameter (2-D thin-plane stress). Generally speaking, a vibration mode of a disk is always of a coupled type [16]. Under certain conditions, the vibrations can be regarded as decoupled, and two-dimensional theory can be used. Although Farag and Pan [16] have found that the coupling effect between the in-plane and thickness modes is noticeable when the ratio of the thickness to the diameter is larger than 0.2 ($h/D > 0.2$). As shown in Fig. 15, the numerical simulation performed for a disk of diameter 29.4 μm and thickness 10 μm shows that (1) can still be used to predict the in-plane resonant frequencies. In addition, the mode shape still follows the formula shown in Part I with good accuracy. This may be explained by that although there exist the accompanying thickness modes [16], the in-plane vibration modes are still dominant for the resonant frequency of interest. Hence, as it was also shown practically, extending the thickness of the disk resonators does not degrade the performance of the device.

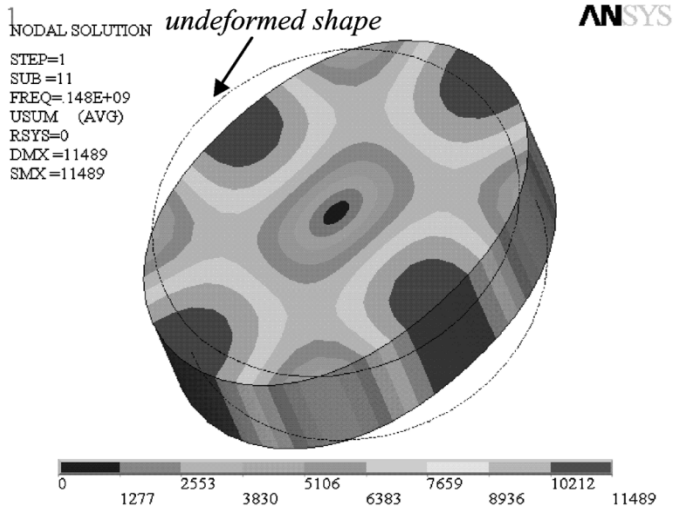

Fig. 15. Elliptic bulk-mode from numerical simulation for a disk of diameter 29.4 μm and thickness 10 μm, supported at its center with isotropic material properties of SCS along the $\langle 110 \rangle$ orientation. Legend shows the displacement distribution across the disk resonator.

V. Summary and Future Directions

Single crystal silicon side-supported disk resonators operating in their elliptical bulk-mode with frequencies in the VHF range were demonstrated. The resonators are actuated and sensed electrostatically with polysilicon electrodes separated from the SCS resonant structure by ultra-narrow capacitive gaps. The resonators are fabricated on SOI substrates and ultra-narrow capacitive transducer gaps are fabricated in a self-aligned manner using a HARPSS-like fabrication process without the need for nanolithography. The ability of fabrication and high-Q operation of thick (18 μm) SCS resonators both under vacuum and in air was demonstrated.

Very high quality factors in the VHF band were achieved by operating the disk resonators in their elliptical bulk-mode. Especially, a quality factor of 46 000 in vacuum at resonance frequency of 149 MHz, which is among the highest reported Q-frequency products (6.8×10^{12}) for micromechanical resonators, was exhibited by an 18-μm-thick disk resonator of 29.2-μm diameter. The resonator was supported by one beam located at one of its resonant nodes. Motional resistance as low as 43.3 kΩ was measured for the same resonator. When operated in atmosphere, the same device demonstrated a Q of 26 000, showing the potential of such devices for several applications without the need for expensive vacuum packaging. A temperature coefficient of frequency of -26 ppm/°C was measured for a 3-μm-thick disk resonator of the same type. The measured electrical tuning slope for the same resonator was -2.6 ppm/V, showing an effective capacitive gap size of 120 nm. The measured characteristics of the resonators were compared to the theoretical analysis presented in Part I, showing good agreement between the measurements and the derived model.

Further reduction of the capacitive gap sizes to deep sub-100 nm range, as well as increasing the device thickness and electrode area will reduce the motional resistance of such resonators to acceptable levels for application as RF components in the VHF and UHF range. In addition, large enough electrostatic frequency-tuning slope for temperature compensation of the resonators can be achieved by reduction of the gap size and maximizing the electrode area.

Acknowledgment

The authors wish to thank G. K. Ho and R. Abdolvand for their contributions and the staff of Georgia Tech Microelectronics Research Center for their assistance.

References

[1] S. Y. No and F. Ayazi, "The HARPSS process for fabrication of nano-precision silicon electromechanical resonators," in *Proc. IEEE Conf. Nanotechnology*, 2001, pp. 489–494. 10/28–30/01.

[2] M. A. Abdelmoneum *et al.*, "Stemless wine-glass-mode disk micromechanical resonators," in *Proc. MEMS'03*, pp. 698–701.

[3] J. Wang *et al.*, "Self-aligned 1.14-GHz vibrating radial mode disk resonators," in *Proc. Transducers'03*, pp. 947–950.

[4] V. T. Srikar and S. D. Senturia, "Thermoelastic damping in fine-grained polysilicon flexural beam resonators," *J. Microelectromech. Syst.*, vol. 11, no. 5, pp. 499–504, Oct. 2002.

[5] V. Kaajakari *et al.*, "Square-extentional mode single-crystal silicon micromechanical RF-resonator," in *Proc. Transducers'03*, pp. 951–954.

[6] S. Humad *et al.*, "High frequency micromechanical piezo-on-silicon block resonators," in *Proc. IEDM'03*, pp. 957–960.
[7] F. Ayazi and K. Najafi, "High aspect-ratio combined poly and single-crystal silicon (HARPSS) MEMS technology," *J. Microelectromech. Syst.*, vol. 9, p. 288, Sept. 2000.
[8] F. Ayazi and K. Najafi, "A HARPSS polysilicon vibrating ring gyroscope," *J. Mech. Syst.*, pp. 169–179, June 2001.
[9] S. Pourkamali and F. Ayazi, "SOI-based HF and VHF single-crystal silicon resonators with sub-100 nm nanometer vertical capacitive gaps," in *Proc. Transducers'03*, pp. 837–840.
[10] S. Y. No, A. Hashimura, S. Pourkamali, and F. Ayazi, "Single crystal silicon HARPSS capacitive resonators with submicron gap spacings," in *Proc. Hilton Head 2002, Solid-State Sensor, Actuator and Microsystems Workshop*, Hilton Head, SC, pp. 281–284.
[11] S. Pourkamali *et al.*, "High-Q single crystal silicon HARPSS capacitive beam resonators with self-aligned sub-100 nm transduction gaps," *J.Microelectromech. Syst.*, pp. 487–496, Aug. 2003.
[12] D. Kobayashi *et al.*, "An integrated lateral tunneling unit," in *Proc. MEMS'92*, pp. 214–219.
[13] J. Wang *et al.*, "1.51 GHz nanocrystalline diamond micromechanical disk resonator with material-mismatched isolating supports," in *Proc. MEMS'04*, pp. 641–644.
[14] S. Pourkamali, R. Abdolvand, and F. Ayazi, "A 600 kHz electrically coupled MEMS bandpass filter," in *Proc. MEMS'03*, 2003, pp. 702–705.
[15] S. Y. Lin, "Coupled vibration and natural frequency analysis of isotropic cylinders or disks of finite dimensions," *J. Sound Vibration*, vol. 185, pp. 193–199, Aug. 1995.
[16] N. H. Farag and J. Pan, "Modal characteristics of in-plane vibration of circular plates clamped at the outer edge," *J. Acoust. Soc. Amer.*, vol. 113, no. 4, pp. 1935–1946, Apr. 2003.

Siavash Pourkamali (S'03) received the B.S. degree in electrical engineering from Sharif University of Technology, Iran, in 2001 and the M.S. degree from Georgia Institute of Technology, Atlanta, in 2004. Currently he is pursuing the Ph.D. degree in Electrical Engineering Department, Georgia Institute of Technology.

His main research interests are in the areas of RF MEMS resonators and filters, silicon micromachining technologies, and integrated microsystems.

Zhili Hao received the B.S. and M.S. degrees in mechanical department from Shanghai Jiao Tong University, Shanghai, P.R. China, in 1994 and 1997, respectively. She received the Ph.D. degree from the University of Central Florida, Department of Mechanical, Materials, and Aerospace Engineering, in 2000. The Ph.D. project was the research and development of a MEMS-based cooling system for microelectronics.

From 2001 to 2002, she worked as a MEMS Engineer with Nanovation Technologies, Inc., Northville, MI, and MEMS Optical, Inc., Huntsville, AL. She was involved in the development of various MEMS products, including electrostatic torsion mirrors, membrane, and piston-type mirrors, microfluidic devices for biomedical and cooling application. She is currently a Postdoctoral Fellow with School of Electrical and Computer Engineering, Georgia Institute of Technology. Her research interests are in the development of MEMS devices and studying fundamental physical mechanisms in MEMS resonant devices, such as support loss and thermoelastic damping.

Dr. Hao is a Member of the American Society of Mechanical Engineers (ASME).

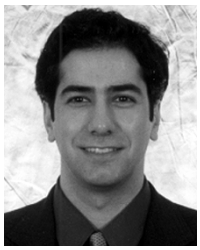

Farrokh Ayazi (S'96–M'99) was born in February 19, 1972. He received the B.S. degree in electrical engineering from the University of Tehran, Iran, in 1994 and the M.S. and the Ph.D. degrees in electrical engineering from the University of Michigan, Ann Arbor, in 1997 and 2000, respectively. He joined the faculty of Georgia Institute of Technology in December 1999, where he is currently an Assistant Professor in the School of Electrical and Computer Engineering. His current research interests are in the areas of low and high frequency micro- and nanoelectromechanical resonators, VLSI analog integrated circuits, MEMS inertial sensors, and microfabrication technologies.

Prof. Ayazi is a 2004 recipient of the NSF CAREER award, the 2004 Richard M. Bass Outstanding Teacher Award, and the Georgia Tech. College of Engineering Cutting Edge Research Award for 2001–2002. He received a Rackham Predoctoral Fellowship from the University of Michigan for 1998–1999.